NJC

Accepted Manuscript

This article can be cited before page numbers have been issued, to do this please use: S. Wang, Y. Liu, Y. Yu, J. Du, Y. Cui, X. Song and Z. Liang, *New J. Chem.*, 2018, DOI: 10.1039/C8NJ01306C.

ROYAL SOCIETY OF CHEMISTRY

rsc.li/njc

View Article Online
DOI: 10.1039/C8NJ01306C

Journal Name

ARTICLE

Conjugated microporous polymers based on biphenylene for CO_2 adsorption and luminescent detection of nitroaromatic compounds†

Received 00th January 20xx,
Accepted 00th January 20xx

DOI: 10.1039/x0xx00000x

www.rsc.org/

Shun Wang,[a] Yuchuan Liu,[a] Yue Yu,[a] Jianfeng Du,[a] Yuanzheng Cui,[a] Xiaowei Song[a,b]* and Zhiqiang Liang[a]*

Conjugated microporous polymers have shown great potential applications in chemosensors, gas storage/separation, light-harvesting and organic electronic materials. In this paper, three novel biphenylene-based conjugated microporous polymers have been synthesized by the palladium-catalyzed Suzuki and Sonogashira-Hagihara cross-coupling reactions of 3,4',5-tribromobiphenyl. N_2 adsorption studies indicate that these polymers are porous, and the BET surface areas are 493, 1576 and 643 $cm^2\ g^{-1}$ for **CMP-LS1–3**, respectively. Amongst these synthesized CMPs, **CMP-LS2** exhibits the highest CO_2 adsorption capacity of 87.4 $cm^3\ g^{-1}$ and reasonable CO_2/N_2 selectivity (27.9) and CO_2/CH_4 selectivity (5.6) at 273 K/1 bar. **CMP-LS1** and **CMP-LS2** exhibit blue luminescence in ethanol suspension. Furthermore, the fluorescence of **CMP-LS1** and **CMP-LS2** can be effectively quenched by PA with the K_{SV} constants of 5.05×10^4 and $3.70 \times 10^4\ M^{-1}$, respectively. They can be used as luminescent sensor for detecting nitroaromatic compounds.

Introduction

Porous organic polymers (POPs), which are composed of light elements (C, H, O, N, B, etc.), have attracted tremendous attention owing to the distinguished features of diverse synthetic methods, high chemical/thermal stability, low skeletal density, easy modification, and high surface area. Large numbers of POPs have been reported including conjugated microporous polymers (CMPs),[1,2] covalent organic frameworks (COFs),[3,4] polymers of intrinsic microporosity (PIMs),[5,6] porous aromatic frameworks (PAFs),[7,8] covalent triazine-based frameworks (CTFs),[9,10] and hypercrosslinked polymers (HCPs),[11-13] etc. POPs, emerging as a promising class of porous materials, have been widely used in the applications of gas storage/separation,[14-16] luminescence,[17,18] catalysis[19-21] and proton conductions[22]. Among porous organic polymers, CMPs combine permanent porosity and high surface areas with conjugated frameworks.[23] Due to their high surface areas and chemical functionality, CMPs have shown great potential for gas adsorption and separation. On the other hand, the extended π-conjugated frameworks of CMPs endow them highly efficient luminescent properties, which have been applied in chemosensors,[24] photocatalysis for hydrogen evolution[25-27] and energy storage.[28]

In recent years, the excessive emission of CO_2 generated by burning fossil fuels brings about global climate change, thus, the capture technology of CO_2 has been garnered increasing interest both in academia and industry. The former process for CO_2 capture is the adsorption based on amine solutions,[29] however, this process suffers from heavy toxicity and high expenditure. Nowadays, adopting solid adsorbents to capture CO_2 has been proved to be an efficient method on account of their mild operating conditions and lower energy penalty.[30] More and more porous materials including zeolites, functional mesoporous SiO_2, metal-organic frameworks (MOFs) and porous organic polymers have been applied into capture and storage of CO_2.[31-34] Besides, stability would be important in many real-life applications. Since first reported in 2007 by Copper et al.,[1] CMPs with permanent porous structures have been extensively investigated for capturing CO_2. The surface area and pore size have a large effect on the gas adsorption and storage performance of CMPs, and it has been proved that the pore properties of CMPs could be adjusted by tuning the monomer length and geometry.[35-37]

Currently, detecting nitroaromatic explosives such as 2,4,6-trinitrotoluene (TNT) and 2,4,6-trinitrophenol (PA) have become one of the most critical issues concerning national security, military applications and environmental safety.[2] During commercial use and production, PA is a non-biodegradable environmental pollutant, which is one kind of strong irritants. Exposed to the air for a long time, PA can cause harm to human health. Luminescent detection method of nitroaromatic explosives came into being owing to its potential merits.[38] In comparison to traditional analysis

[a] State Key Lab of Inorganic Synthesis and Preparative Chemistry, College of chemistry, Jilin University, Changchun, 130012, P. R. China,
E-mail: liangzq@jlu.edu.cn; xiaoweisong@jlu.edu.cn
[b] Department of Physical and Macromolecular Chemistry, Faculty of Science, Charles University in Prague, 128 43 Prague 2, Czech Republic

† Electronic Supplementary Information (ESI) available: ^{1}H NMR spectra, IR, PXRD, TGA, SEM, UV-vis and fluorescence spectra, gas adsorption and selectivity for **CMP-LS1–3**. See DOI: 10.1039/x0xx00000x.

View Article Online
DOI: 10.1039/C8NJ01306C

methods, such as gas chromatography, liquid chromatography-mass spectrometry and spectrophotography, luminescence-based detection possesses a plenty number of nonnegligible advantages, including high sensitivity, simplicity, short response time, low expense, as well as it can be tested in both solution and solid phase.[39] Numbers of π-electron-rich fluorescent conjugated polymers have been successfully synthesized and reported as chemosensors, especially, luminescent CMPs are widely employed in detection of nitroaromatic compounds.[40,41]

In this paper, we report the synthesis of three polyphenylene conjugated microporous polymers (**CMP-LS1–3**) via Pd-catalyzed Suzuki and Sonogashira-Hagihara cross-coupling reactions of 3,4',5-tribromobiphenyl and comonomers such as 1,3,5-tris(4,4,5,5-tetramethyl-1,3,2-dioxaborolan-2-yl)benzene, 1,4-phenylenediboronic acid and 1,3,5-triethynylbenzene (Scheme 1). Of all the polymers investigated, **CMP-LS2** exhibits high Brunauer–Emmett–Teller (BET) surface areas up to 1576 $m^2 g^{-1}$ and good CO_2 uptake up to 87.4 $cm^3 g^{-1}$ at 273 K and 1.0 bar. The CO_2 selectivity of **CMP-LS1–3** over CH_4 was calculated to be 4.5, 5.6, 4.5 at 273 K and 1.0 bar (CO_2/CH_4, 5/95), and **CMP-LS1–3** exhibits the CO_2/N_2 selectivity of 23.2, 27.9, 19.8 at 273 K and 1.0 bar (CO_2/N_2, 15/85). Besides, the resulting two luminescent polymers (**CMP-LS1** and **CMP-LS2**) show high selective and sensitive detection ability of PA in suspension of ethanol.

Experimental Section

Materials

Unless otherwise noted, all reagents were purchased from commercial suppliers and used without further purification. 3,4',5-Tribromobiphenyl was synthesized via Pd-catalyzed Suzuki reaction of 1-bromo-4-iodobenzene and 3,5-dibromobenzeneboronic acid.

Characterization

Powder X-ray diffraction (PXRD) patterns were collected on a Rigaku D-Max 2550 diffractometer using Cu-Kα radiation (λ = 0.15418 nm) in a 2θ range of 4–40° at room temperature. Fourier transform infrared (FTIR) spectra were recorded in the range of 400–4000cm^{-1} on a Nicolet 6700 FT-IR spectrometer with KBr pellets. Thermogravimetric analyses (TGA) were performed on a Perkin-Elmer TGA-7 thermogravimetric analyzer from room temperature to 800 °C in air atmosphere with a heating rate of 10 °C/min. Scanning electron microscopy (SEM) was performed on a JSM-6700F electron microscope. Fluorescence spectra were recorded on a FLUOROMAX-4 fluorescence spectrophotometer. ^{1}H NMR and ^{13}C NMR spectra were recorded at room temperature using a Varian Mercury spectrometer operating at frequencies of 300 and 75 MHz for ^{1}H and ^{13}C, respectively. The solid-state ^{13}C cross-polarization/magic-angle spinning (CP/MAS) NMR spectra were collected a Bruker AVANCE III 400 WB spectrometer. All gases adsorption-desorption measurements at different temperature were carried out on a Micromeritics ASAP 2020 instrument. The samples were degassed at 100 °C under vacuum for 10 h.

Synthesis of 3,4',5-tribromobiphenyl (TBBP)

A mixture of 1-bromo-4-iodobenzene (2.83 g, 10 mmol), 3,5-dibromobenzeneboronic acid (2.80 g, 10 mmol), $Pd(PPh_3)_4$ (578 mg, 0.5 mmol) and anhydrous K_2CO_3 (8.28 g, 60 mmol) was placed into a Schlenk reaction tube (200 mL) equipped with a magnetic stirring bar under N_2 atmosphere. Then 100 mL DMF was added to the reaction tube. The resulting solution was degassed and purged with nitrogen three times. After being heated at 85 °C for 12 h under a nitrogen atmosphere, the reaction mixture was quenched with water, extracted with ethyl acetate, washed with brine, dried over $MgSO_4$. The collected organic phase was concentrated by a rotary evaporator and the crude product was purified by silica-gel column with petroleum ether as eluent. **TBBP** was obtained as a white solid in 53% yield (2.07 g). ^{1}H NMR ($CDCl_3$, 300 MHz): δ (ppm) 7.68–7.55 (m, 5H), 7.42–7.36 (m, 2H). ^{13}C NMR ($CDCl_3$, 75 MHz): δ (ppm) 143.4, 137.1, 132.9, 132.1, 128.7, 128.5, 123.3, 122.9 (Fig. S1 and S2).

Synthesis of CMP-LS1

A mixture of **TBBP** (391 mg, 1 mmol), 1,4-phenylenediboronic acid (249 mg, 1.5 mmol), anhydrous K_2CO_3 (827 mg, 6 mmol) and $Pd(PhCN)_2Cl_2$ (19 mg, 0.05 mmol) were dissolved in DMF (40 mL). The reaction mixture was heated at 120 °C and stirred for 60 h under N_2 atmosphere. The mixture was cooled to room temperature, and quenched by addition of water. The precipitated polymer was collected by filtration and washed several times with water, methanol, and acetone to remove any unreacted monomers or catalyst residues. Then further purification of the polymer was washed by Soxhlet extraction with methanol and THF for 24 h each. The solid was dried in a vacuum oven for 12 h at 50 °C to obtain **CMP-LS1** as gray-black powder (218 mg, yield: 82%).

Synthesis of CMP-LS2

CMP-LS2 was synthesized employing the similar steps as described for **CMP-LS1**. **TBBP** (391 mg, 1 mmol), 1,3,5-tris(4,4,5,5-tetramethyl-1,3,2-dioxaborolan-2-yl)benzene (456 mg, 1 mmol) were used for this polymerization. **CMP-LS2** was collected as gray-black powder (178 mg, yield: 79%).

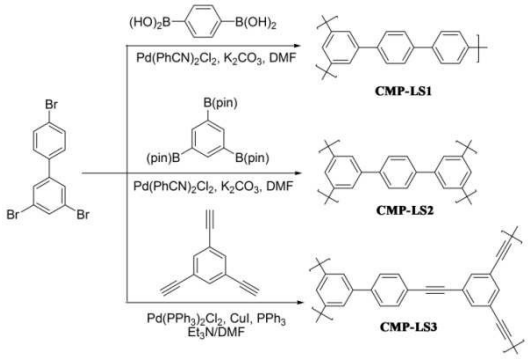

Scheme 1 Synthetic routes of **CMP-LS1–3**.

View Article Online
DOI: 10.1039/C8NJ01306C
Journal Name ARTICLE

Synthesis of CMP-LS3

TBBP (313 mg, 0.8 mmol), 1,3,5-triethynylbenzene (118 mg, 0.8 mmol), $Pd(PPh_3)_2Cl_2$ (28 mg, 0.04 mmol), copper(I) iodide (15 mg, 0.08 mmol) and PPh_3 (21 mg, 0.08 mmol) were dissolved in a mixture of anhydrous DMF (20 mL) and Et_3N (20 mL). Then the following steps were same to the synthesis of **CMP-LS1**. **CMP-LS3** was obtained as brown powder (213 mg, yield: 90%).

Results and Discussion

Synthesis of CMP-LS1–3

As shown in Scheme 1, **CMP-LS1–3** were synthesized from 3,4',5-tribromobiphenyl through palladium catalyzed Suzuki and Sonogashira-Hagihara coupling reactions. For **CMP-LS1** and **CMP-LS2**, the Suzuki reactions of 3,4',5,-tribromobiphenyl with 1,4-phenylenediboronic acid or 1,3,5-tris(4,4,5,5-tetramethyl-1,3,2-dioxaborolan-2-yl)benzene were conducted in the catalytic system of $Pd(PhCN)_2Cl_2/K_2CO_3$/DMF at 120 °C for 60 h. While for **CMP-LS3**, the Sonogashira-Hagihara reaction of 3,4',5,-tribromobiphenyl with 1,3,5-triethynylbenzene was performed in the catalytic system of $Pd(PPh_3)_2Cl_2$/CuI/PPh_3/DMF/Et_3N at 120 °C for 60 h. All these polymers are formed as fine powder and insoluble in the general organic solvents such as DMF, DMSO, CH_2Cl_2 and THF.

Characterization of CMP-LS1–3

Thermogravimetric analyses (TGA) of **CMP-LS1–3** show their excellent thermal stability and high decomposition temperatures under air atmosphere. As shown in Fig. S3, **CMP-LS1–3** are stable up to 320–400 °C, respectively. It should be mentioned is that the high stabilities make many potential applications available. Powder X-ray diffraction measurements show that their textures are amorphous (Fig. S4). Meanwhile, scanning electron microscopy (SEM) was carried out to collect the morphology information of CMPs (Fig. S5). The SEM images indicate that all the polymers have irregular shapes.

The formation of the CMPs skeleton was initially characterized through Fourier transform infrared (FT-IR) spectroscopy (Fig. S6). In the FT-IR spectrum of TBBP, the characteristic vibration of C-Br band is obviously observed at around 560 cm^{-1}, while it became very weak in the FT-IR spectra of **CMP-LS1–3**. Furthermore, the typical -C≡C- stretching mode at about 2200 cm^{-1} is observed in **CMP-LS3**. These results indicate that the desired polymers have been obtained. The frameworks of **CMP-LS1–3** were further investigated by solid-state ^{13}C CP/MAS NMR spectroscopy (Fig. 1). For **CMP-LS1** and **CMP-LS2**, the solid-state ^{13}C CP/MAS NMR spectra exhibit only two main peaks at around 141 and 127 ppm, which could be assigned as the substituted and non-substituted aromatic carbons, respectively. While for **CMP-LS3**, there are several signals between 140 and 124 ppm corresponding to the aromatic carbons of different benzene rings in the framework. The additional broad peak at about 90 ppm corresponds to ethynylene bonds of **CMP-LS3**. The less

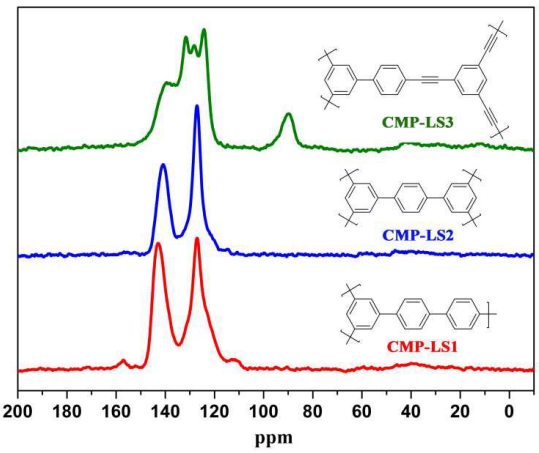

Fig. 1 The solid-state ^{13}C CP/MAS NMR spectra of **CMP-LS1–3**.

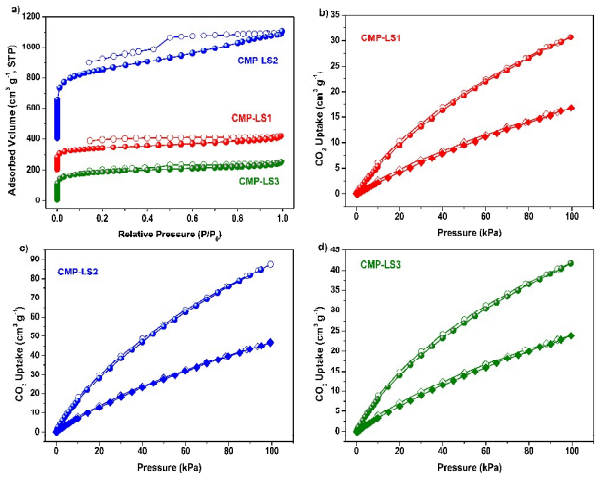

Fig. 2 (a) N_2 sorption isotherms at 77 K and CO_2 sorption isotherms of **CMP-LS1** (b), **CMP-LS2** (c), **CMP-LS3** (d) collected at 273 K (cycle) and 298 K (square).

Table 1 Porosity properties of **CMP-LS1-3**

Sample	S_{BET} ($m^2\ g^{-1}$)	V_{total} ($cm^3\ g^{-1}$)	V_{micro} ($cm^3\ g^{-1}$)	CO_2 Uptake[a] ($cm^3\ g^{-1}$)	Isosteric heats/kJ mol^{-1}
CMP-LS1	493	0.32	0.12	31/17	30.2
CMP-LS2	1576	1.06	0.36	87/47	31.6
CMP-LS3	643	0.37	0.17	42/24	30.4

[a] Measured at a pressure of 1 bar at 273/298 K.

aromatic carbon signals of **CMP-LS1** and **CMP-LS2** than those of **CMP-LS3** indicate the higher symmetry of benzene rings in the frameworks of **CMP-LS1** and **CMP-LS2**.

Porosity properties and gas adsorption studies of CMP-LS1–3

The nitrogen gas adsorption and desorption isotherms at 77 K were performed to investigate the porosity properties of **CMP-LS1–3**. As shown in Fig. 2a, these CMPs exhibited rapid uptake of N_2 at a relatively low pressure ($P/P_o < 0.05$) and followed by

View Article Online
DOI: 10.1039/C8NJ01306C

a slow increase. According to the IUPAC classification, they exhibit Type I nitrogen gas sorption isotherms with H4 type hysteresis loops. The BET surface areas were calculated within the relative pressure (P/P_o) range from 0.05 to 0.20, which generates apparent surface areas of 493, 1576 and 643 $m^2 g^{-1}$ for **CMP-LS1–3**, respectively. The pore size distributions (PSDs) of CMPs based on the non-local density functional theory (NLDFT) method display the main peaks at 0.4–1.4 nm, confirming their predominant microporous structures (Fig. S7). In addition, **CMP-LS2** shows some mesoporous, which is consistent with the N_2 sorption isotherm. The total pore volume (V_{total}) estimated from the single point measurement of the N_2 uptake at P/P_o = 0.97 is 0.32, 1.06 and 0.37 $cm^3 g^{-1}$ for **CMP-LS1–3**, and the micropore volume (V_{micro}) is 0.12, 0.36 and 0.17 $cm^3 g^{-1}$, respectively. Detailed porosity data for the CMPs in this study are compiled in Table 1.

Furthermore, we measured the CO_2 sorption isotherms of **CMP-LS1–3** from low pressure to 1.0 bar at 273 K and 298 K to further study their potential application in CO_2 capture. As shown in Fig. 2b–d. Of all the polymers investigated, **CMP-LS2** exhibited the highest CO_2 uptake up to 87.4 $cm^3 g^{-1}$ at 273 K and 46.7 $cm^3 g^{-1}$ at 298 K, respectively, which are comparable to most of the reported POPs under similar conditions (Table S1). The CO_2 uptakes of **CMP-LS1** and **CMP-LS3** are 30.7 and 41.6 $cm^3 g^{-1}$ CO_2 at 273 K, 16.7 and 23.7 $cm^3 g^{-1}$ at 298 K, respectively. Generally, sorbents with high surface areas also have relatively high CO_2 adsorption under the same conditions. Moreover, the structure and special groups also have an effect on the capture capacity of CO_2.[42] To investigate the binding affinity of **CMP-LS1–3** towards CO_2, we calculated the isosteric heats of adsorption (Q_{st}) using adsorption data measured at 273 K and 298 K by the Clausius–Clapeyron equation. As shown in Fig. S8, the isosteric heats of **CMP-LS1**, **CMP-LS2** and **CMP-LS3** at zero coverage are 33.6, 36.6 and 35.3 kJ mol^{-1}, respectively.

The separation abilities of these three CMPs for different gases at 273 K have also been studied. N_2 and CH_4 sorption isotherms were recorded at 273 K (Fig. 3). The CH_4 and N_2 uptakes at 273 K and 1 bar are 10.38 and 2.47 $cm^3 g^{-1}$ for **CMP-LS1**, 27.22 and 6.54 $cm^3 g^{-1}$ for **CMP-LS2**, 15.70 and 2.82 $cm^3 g^{-1}$ for **CMP-LS3**, respectively. These values are much lower than those of CO_2 (30.7, 87.4 and 41.6 $cm^3 g^{-1}$). To evaluate the CO_2/CH_4 and CO_2/N_2 selectivities of **CMP-LS1–3** under mixture gas conditions with single component isotherms at 273 K, the ideal adsorbed solution theory (IAST) could be used to predict the multicomponent adsorption behaviors under the conditions of 5% CO_2 balanced with 95% CH_4, the IAST adsorption selectivity for **CMP-LS1–3** is calculated to be 4.5, 5.6, 4.5 at 273 K and 1.0 bar (Fig. 3d, Fig. S9 and Table S2). Furthermore, the CO_2 selectivity of **CMP-LS1–3** over N_2 was also calculated. Under simulated flue gas conditions (CO_2/N_2, 15/85), **CMP-LS1–3** exhibit the CO_2-over-N_2 selectivity of 23.2, 27.9, 19.8 at 273 K and 1.0 bar (Fig. 3d). In addition, the selectivities of **CMP-LS1–3** for CO_2/CH_4 and CO_2/N_2 are comparable to other POPs (Table S3). These performances exhibit that **CMP-LS1–3** can be used as promising materials in gas storage and separation.

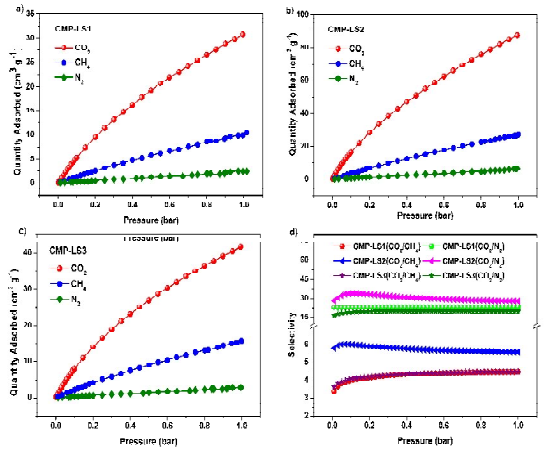

Fig. 3 CO_2, CH_4, and N_2 adsorption isotherms of **CMP-LS1** (a), **CMP-LS2** (b) and **CMP-LS3** (c) at 273 K. CO_2/CH_4 and CO_2/N_2 selectivity of **CMP-LS1-3** (d) for a molar ratio of 5/95 and 15/85 at 273 K.

Luminescent properties

The UV-vis absorption spectra of **CMP-LS1–2** in ethanol show absorption peaks at 335 and 271 nm (Fig. S10). Due to the presence of full π-conjugated skeleton derived from the connection of all phenyl rings, **CMP-LS1** and **CMP-LS2** exhibit a strong luminescence in ethanol suspension at 413 nm and 385 nm (λ_{ex} = 345 and 332 nm (Fig. S11).

The strong luminescence of **CMP-LS1** and **CMP-LS2** inspired us to explore their potential applications in the detection of nitroaromatic compounds. The luminescent sensing properties of **CMP-LS1** and **CMP-LS2** were investigated in ethanol suspensions. 2,4-Dinitrotoluene (DNT), 4-nitrotoluene (NT), 4-nitrobenzaldehyde (NBA), 4-chloronitrobenzene (ClNB), 1-chloro-2,4-dinitrobenzene (ClDNB), 4-nitrophenol (NP) and picric acid (PA) were added to ethanol suspensions of **CMP-LS1** and **CMP-LS2** to explore luminescent quenching percentage. The luminescent quench percentage (QP) was calculated with the equation of QP = $[(I_o - I)/I_o] \times 100\%$ (Fig. 4). The two polymers display low sensing ability towards DNT, NT, NP, NBA, ClNB and ClDNB in the systems (Fig. S12 and S13). However, they show highly sensitive sensing ability towards PA, and the fluorescence emission maximum was nearly instantaneously reduced upon the addition of PA in a relatively short time. The fluorescence intensities of **CMP-LS1** and **CMP-LS2** suspensions were quenched to 81% and 83% by increasing the concentration of PA to 47.6 μM and 56.6 μM (Fig. 5a and 5b) (Fig. S14). The quenching efficiency of PA can be analyzed using the Stern-Volmer (SV) equation: $I_o/I = 1 + K_{SV} \times [M]$. The S–V plots for PA of **CMP-LS1** and **CMP-LS2** are almost linear at low concentrations (Fig. 5c and 5d). The quenching constants for PA are found to be 5.05×10^4 M^{-1} and 3.70×10^4 M^{-1} for **CMP-LS1** and **CMP-LS2**, respectively, which are comparable to other reported polymers chemosensors in the literatures (Table S4). In addition, the recyclability of **CMP-LS1** and **CMP-LS2** for PA detection have been carried out. The used samples can be regenerated after simple centrifugation and washing three times with ethanol (Fig. 6).

View Article Online
DOI: 10.1039/C8NJ01306C

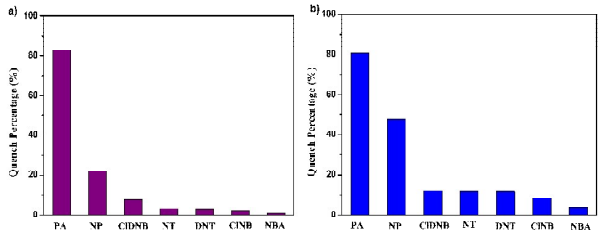

Fig. 4 Reduction of luminescence intensities of **CMP-LS1** (a) and **CMP-LS2** (b) in the presence of different nitroaromatic explosives with the concentration of 47.6 and 56.6 μM.

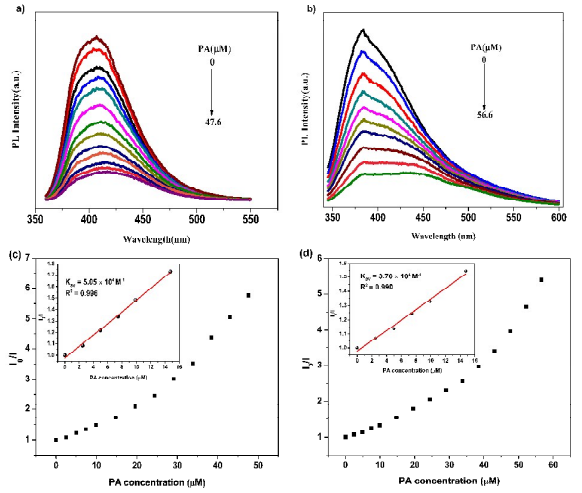

Fig. 5 Emission quenching observed for the suspension of **CMP-LS1** (a) and **CMP-LS2** (b) (0.25 mg mL^{-1} in ethanol, λ_{ex} = 345 and 332 nm) upon addition of nitroaromatic compounds. The relationship of I_0/I with PA concentration in ethanol suspensions of **CMP-LS1** (c) and **CMP-LS2** (d); (insets: Stern–Volmer plots at low PA concentrations).

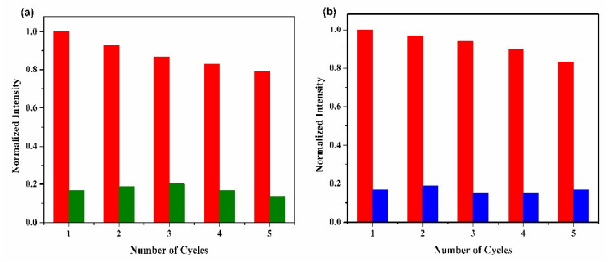

Fig. 6 The quenching and recovery test of **CMP-LS1** and **CMP-LS2** (0.25 mg ml^{-1}) dispersed in ethanol in the presence of PA solution (the red bars represent the initial fluorescence intensities, and the olive and blue bars represent the intensities after the addition of PA (47.6 and 56.6 μM) for **CMP-LS1** and **CMP-LS2**, respectively).

Generally, the fluorescence quenching phenomenon can be explained by the donor-acceptor electron-transfer mechanism through the interaction between electron-rich CMPs and electron-deficient nitro analytes.[43] The conduction band (CB) of the electron-rich CMPs lies higher than the LUMO energies of the nitro analytes and upon excitation the excited electron from the CB transfers to the LUMO orbitals of the nitro analytes, thus quenching the fluorescence intensity. However, the electron transfer is not the only mechanism contributing to fluorescence quenching.[44] the fluorescence quenching phenomenon can be explained by the resonance energy transfer mechanism.[45,46] The resonance energy transfer could occur from fluorophore to non-emissive analyte, if the analyte and fluorophore are close to each other and the absorption spectrum of the analyte has an effective overlap with the emission spectrum of the fluorophore. The greater the spectral spectrum overlap between the absorbance spectrum of the analyte and the emission spectrum of the CMPs, the higher the probability of energy transfer.[47] The UV-vis absorption spectra of these nitroaromatic compounds were compared with the luminescent spectra of **CMP-LS1** and **CMP-LS2**. As shown in Fig. S15, the greatest spectral overlap is between PA and the CMPs, and overlaps occur to some extent in NP/CMPs, while there are no spectral overlaps between other nitro compounds and CMPs. Thus, PA has the greatest quenching of the fluorescence for the **CMP-LS1** and **CMP-LS2**, which could be promising candidates for practical PA sensing.

Conclusions

In summary, three biphenylene-based CMPs have been synthesized via palladium-catalyzed Suzuki and Sonogashira-Hagihara polycondensation of 3,4',5-tribromobiphenyl. These polymers are mainly microporous materials and show better CO_2 absorption capacities. At 273 K and 1.0 bar, **CMP-LS2** exhibits the highest CO_2 uptake of 87 cm^3 g^{-1}. In addition, all of the polymers show good separation ability for CO_2-over-N_2 and CO_2-over-CH_4. These properties suggest that **CMP-LS1–3** can be adopted as promising materials in gas storage and separation. Furthermore, owing to π-conjugated skeleton and the rigid microporous environment, **CMP-LS1** and **CMP-LS2** exhibit high sensitive and selective fluorescence quenching to PA with the SV constant of 5.05×10^4 M^{-1} and 3.70×10^4 M^{-1}. In terms of environment and security concerns, the present work suggests that these materials may be fluorescence sensor of PA.

Conflicts of interest

There are no conflicts to declare.

Acknowledgements

We thank the National Natural Science Foundation of China (Grants: 21471064, 21641004 and 21621001), the "111" project of the Ministry of Education of China (B17020) and OP VVV "Excellent Research Teams", project NO. CZ.02.1.01/0.0/0.0/15_003/0000417–CUCAM for support to this work.

Notes and references

1 J. X. Jiang, F. Su, A. Trewin, C. D. Wood, N. L. Campbell, H. Niu, C. Dickinson, A. Y. Ganin, M. J. Rosseinsky, Y. Z. Khimyak and A. I. Cooper, *Angew. Chem., Int. Ed.*, 2007, **46**, 8574–8578.

View Article Online
DOI: 10.1039/C8NJ01306C

2 Y. Xu, S. Jin, H. Xu, A. Nagai and D. Jiang, *Chem. Soc. Rev.*, 2013, **42**, 8012–8031.
3 X. Feng, X. Ding and D. Jiang, *Chem. Soc. Rev.*, 2012, **41**, 6010–6022.
4 M. Matsumoto, R. R. Dasari, W. Ji, C. H. Feriante, T. C. Parker, S. R. Marder and W. R. Dichtel, *J. Am. Chem. Soc.*, 2017, **139**, 4999–5002.
5 N. B. McKeown, *Sci. China Chem*. 2017, **60**, 1023-1032.
6 B. S. Ghanem, K. J. Msayib, N. B. McKeown, K. D. M. Harris, Z. Pan, P. M. Budd, A. Butler, J. Selbie, D. Book and A. Walton, *Chem. Commun.*, 2007, 67-69.
7 U. Díaz and A. Corma, *Coordin. Chem. Rev.*, 2016, **311**, 85-124.
8 D. Yuan, W. Lu, D. Zhao and H.-C. Zhou, *Adv. Mater.*, 2011, **23**, 3723–3725.
9 P. Puthiaraj, Y.-R. Lee, S. Zhang and W.-S. Ahn, *J. Mater. Chem. A*, 2016, **4**, 16288-16311.
10 P. Katekomol, J. Roeser, M. Bojdys, J. Weber and A. Thomas, *Chem. Mater.*, 2013, **25**, 1542–1548.
11 L. Tan and B. Tan, *Chem. Soc. Rev.*, 2017, **46**, 3322-3356.
12 S. Xu, Y. Luo and B. Tan, *Macromol. Rapid Commun.*, 2013, **34**, 471–484.
13 J. Zhang, Z.-A. Qiao, S. M. Mahurin, X. Jiang, S.-H. Chai, H. Lu, K. Nelson and S. Dai, *Angew. Chem., Int. Ed.*, 2015, **54**, 4582–4586.
14 Q. Song, S. Jiang, T. Hasell, M. Liu, S. Sun, A. K. Cheetham, E. Sivaniah and A. I. Cooper, *Adv. Mater.*, 2016, **28**, 2629–2637.
15 Z.-A. Qiao, S.-H. Chai, K. Nelson, Z. Bi, J. Chen, S. M. Mahurin, X. Zhu and S. Dai, *Nat. Commun.*, 2014, **5**, 3705.
16 Y. F. Chen, H. X. Sun, R. X. Yang, T. T. Wang, C. J. Pei, Z. T. Xiang, Z. Q. Zhu, W. D. Liang, A. Li and W. Q. Deng, *J. Mater. Chem. A*, 2015, **3**, 87–91.
17 L. Sun, Z. Liang, J. Yu and R. Xu, *Polym. Chem.*, 2013, **4**, 1932–1938.
18 Y. Cui, Y. Liu, J. Liu, J. Du, Y. Yu, S. Wang, Z. Liang and J. Yu, *Polym. Chem.*, 2017, **8**, 4842–4848.
19 P. Kaur, J. T. Hupp and S. T. Nguyen, *ACS Catal.*, 2011, **1**, 819–835.
20 Y.-B. Zhou, Y.-Q. Wang, L.-C. Ning, Z.-C. Ding, W.-L. Wang, C.-K. Ding, R.-H. Li, J.-J. Chen, X. Lu, Y.-J. Ding and Z.-P. Zhan, *J. Am. Chem. Soc.*, 2017, **139**, 3966–3969.
21 S. Hao, Y. Liu, C. Shang, Z. Liang and J. Yu, *Polym. Chem.*, 2017, **8**, 1833–1839.
22 H. Ma, B. Liu, B. Li, L. Zhang, Y.-G. Li, H.-Q. Tan, H.-Y. Zang and G. Zhu, *J. Am. Chem. Soc.*, 2016, **138**, 5897–5903.
23 S. Ren, R. Dawson, A. Laybourn, J.-x. Jiang, Y. Khimyak, D. J. Adams and A. I. Cooper, *Polym. Chem.*, 2012, **3**, 928–934.
24 Y. Xu, L. Chen, Z. Guo, A. Nagai and D. Jiang, *J. Am. Chem. Soc.*, 2011, **133**, 17622–17625.
25 R. S. Sprick, J.-X. Jiang, B. Bonillo, S. Ren, T. Ratvijitvech, P. Guiglion, M. A. Zwijnenburg, D. J. Adams and A. I. Cooper, *J. Am. Chem. Soc.*, 2015, **137**, 3265–3270.
26 C. Yang, B. C. Ma, L. Zhang, S. Lin, S. Ghasimi, K. Landfester, K. A. I. Zhang and X. Wang, *Angew. Chem., Int. Ed.*, 2016, **55**, 9202–9206.
27 Y. Xu, N. Mao, C. Zhang, X. Wang, J. Zeng, Y. Chen, F. Wang, J.-X. Jiang, *Appl. Catal. B: Environ.*, 2018, **228**, 1-9.
28 C. Zhang, Y. He, P. Mu, X. Wang, Q. He, Y. Chen, J. Zeng, F. Wang, Y. Xu, J.-X. Jiang, *Adv. Funct. Mater.*, 2018, **28**, 1705432.
29 F. Li and L.-S. Fan, *Energy Environ. Sci.*, 2008, **1**, 248–267.
30 D. M. D'Alessandro, B. Smit and J. R. Long, *Angew. Chem., Int. Ed.*, 2010, **49**, 6058–6082.
31 F. Su, C. Lu, S.-C. Kuo and W. Zeng, *Energy Fuels*, 2010, **24**, 1441–1448.
32 R. Kishor and A. K. Ghoshal, *Microporous and Mesoporous Mater.*, 2017, **246**, 137–146.
33 K. Sumida, D. L. Rogow, J. A. Mason, T. M. McDonald, E. D. Bloch, Z. R. Herm, T.-H. Bae and J. R. Long, *Chem. Rev.*, 2012, **112**, 724–781.
34 R. Dawson, E. Stöckel, J. R. Holst, D. J. Adams and A. I. Cooper, *Energy Environ. Sci.*, 2011, **4**, 4239–4245.
35 J. Schmidt, M. Werner and A. Thomas, *Macromolecules*, 2009, **42**, 4426–4429.
36 L. Qin, G.-J. Xu, C. Yao and Y.-H. Xu, *Chem. Commun.*, 2016, **52**, 12602–12605.
37 J.-X. Jiang, F. Su, A. Trewin, C. D. Wood, H. Niu, J. T. A. Jones, Y. Z. Khimyak and A. I. Cooper, *J. Am. Chem. Soc.*, 2008, **130**, 7710–7720.
38 L. Sun, Z. Liang and J. Yu, *Polym. Chem.*, 2015, **6**, 917–924.
39 T.-M. Geng, S.-N. Ye, Y. Wang, H. Zhu, X. Wang and X. Liu, *Talanta*, 2017, **165**, 282–288.
40 L. Sun, Y. Zou, Z. Liang, J. Yu and R. Xu, *Polym. Chem.*, 2014, **5**, 471–478.
41 T.-M. Geng, D.-K. Li, Z.-M. Zhu, Y.-B. Guan and Y. Wang, *Microporous and Mesoporous Mater.*, 2016, **231**, 92–99.
42 O. Buyukcakir, S. H. Je, D. S. Choi, S. N. Talapaneni, Y. Seo, Y. Jung, K. Polychronopoulou and A. Coskun, *Chem. Commun.*, 2016, **52**, 934–937.
43 S. J. Toal and W. C. Trogler, *J. Mater. Chem.*, 2006, **16**, 2871–2883.
44 H. Ma, B. Li, L. Zhang, D. Han and G. Zhu, *J. Mater. Chem. A*, 2015, **3**, 19346–19352.
45 J. C. Sanchez, A. G. DiPasquale, A. L. Rheingold and W. C. Trogler, *Chem. Mater.*, 2007, **19**, 6459–6470.
46 S. S. Nagarkar, A. V. Desai and S. K. Ghosh, *Chem. Commun.*, 2014, **50**, 8915–8918.
47 S. S. Nagarkar, B. Joarder, A. K. Chaudhari, S. Mukherjee and S. K. Ghosh, *Angew. Chem., Int. Ed.*, 2013, **52**, 2881–2885.

View Article Online
DOI: 10.1039/C8NJ01306C

Table of contents

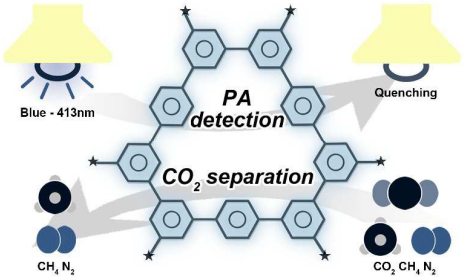

Conjugated microporous polymers based on biphenylene exhibit selective adsorption CO_2 over CH_4 and N_2, and luminescent sensing for picric acid.